Point Slits Versus Linear Slits in the Angular Correlation of Positron Annihilation Radiation.

P. Colombino, B. Fiscella and L. Trossi (*)

Istituto di Fisica dell'Università - Torino
Istituto Nazionale di Fisica Nucleare - Sezione di Torino

(ricevuto il 25 Luglio 1962)

Summary. — A new experimental apparatus has been used to study the angular distribution of γ-rays from positron annihilation. The coincidence counting rate $N_z(p_z)$ is proportional to a linear integral of the momentum density function, while with the previous experimental set up it was proportional to a double integral. The results of measurements carried out on various oriented samples of graphite are discussed.

1. – Introduction.

The angular correlation of positron annihilation radiation in solids and liquids was studied by many authors using a technique introduced by De Benedetti and Lang [1].

Until now such a technique has been employed, with few exceptions [2,3], in the study of amorphous and polycrystalline substances: from such materials one can obtain information only on the mean spherical value of the electron momentum.

In the present paper we describe a new geometry which we think very convenient for the study of oriented crystals. Moreover the possibility of

(*) A significant part of this work is due also to Doctor I. Degregori, now at L.R.S.R. (Milano).

(1) L. G. Lang and S. De Benedetti: *Phys. Rev.*, **108**, 914 (1957).

(2) S. Berko, R. E. Kelley and J. S. Plaskett: *Phys. Rev.*, **106**, 824 (1958).

(3) S. Berko and J. S. Plaskett: *Phys. Rev.*, **112**, 1877 (1958).

observing details of the Fermi surface in conducting crystals by means of this geometry, does not seem unreasonable, provided the crystals are oriented along suitable directions with respect to the measuring apparatus.

2. – Experimental apparatus.

The usual experimental set-up which has been already used for our previous measurements (4) consists substantially of two scintillating crystals, S_1, S_2, in coincidence, Fig. 1*a*, placed two meters apart at opposite sides of the sample target, and detecting the γ-rays arising from the target.

The scintillators are protected by linear collimating slits, 2 mm wide and extended 150 mm in the Y direction, normal to the propagation of γ-rays (X-axis). One of the counters is fixed, while the other, mounted on an arm, can move in the Z direction by rotating upon an angle ϑ about an axis passing through the sample and parallel to Y.

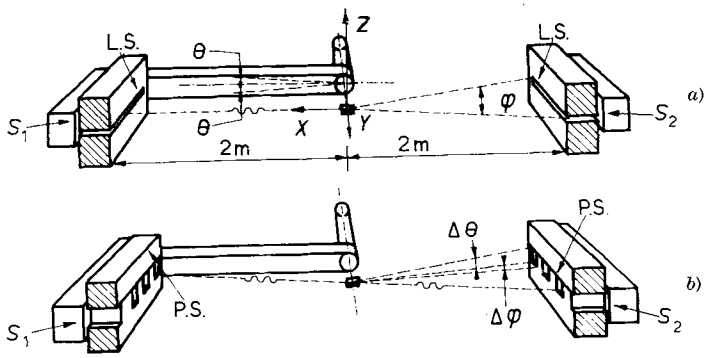

Fig. 1. – Schematic disposition of linear (*a*) and point (*b*) slits.

The coincidence counting-rate $N_z(p_z)$ recorded by such an apparatus at an angle ϑ, is proportional to the probability that the p_z component of the total momentum of the annihilating pair falls between p_z and $p_z + \mathrm{d}p_z$.

$N_z(p_z)$ depends on a double integral of the momentum density function $\chi\chi^*(p_x, p_y, \vartheta mc)$ of the electron, that is,

$$N_z(p_z) \propto \iint_{\infty} \chi\chi^* \,\mathrm{d}p_x \,\mathrm{d}p_y \,, \tag{1}$$

where $p_z = \vartheta mc$.

(4) P. COLOMBINO, I. DEGREGORI, L. MAIRONE, L. TROSSI and S. DEBENEDETTI: *Nuovo Cimento*, **18**, 632 (1960).

From eq. (1) we can see that if $N_z(p_z)$ must be independent of p_y, the slits must be infinitely extended in the Y direction; in this case the angle φ subtending the slit aperture from the sample target, must be equal to π. In practice an angle $\varphi \simeq 0.1$ rad is more than sufficient, since the deviation of annihilating γ-rays from true antiparallelism reaches at most the value of $15 \cdot 10^{-3}$ rad.

With slits of 150 mm of length ($\varphi = 7.5 \cdot 10^{-2}$ rad), this condition is widely fulfilled: as a matter of fact it can be easily seen that a γ-ray entering, for instance, in the center of one of the slits, allows the other γ-ray to fall at most at ± 30 mm from the middle of the other slit.

We shall use of this fact as it will be shown later.

From (1) we can notice that $N_z(p_z)$ depends on a surface integral: since our aim is to get information on $\chi\chi^*(\boldsymbol{p})$ or $N(p)$, we could obtain more details by replacing the described geometry by a different improved geometry, Fig. 1*b*, which gives a dependence on a line integral.

We can do this by restricting the slits to point apertures, *i.e.* by reducing the angle φ to a value $\Delta\varphi$ of the same order of $\Delta\vartheta$.

We have then:

$$mc\left(\theta - \frac{\Delta\theta}{2}\right) \leqslant p_z \leqslant mc\left(\theta + \frac{\Delta\theta}{2}\right),$$

$$-mc\frac{\Delta\varphi}{2} \leqslant p_y \leqslant +mc\frac{\Delta\varphi}{2},$$

$$-\infty \leqslant p_x \leqslant +\infty,$$

and the resulting counting rate in this case is

$$n_z(p_z) \propto \int_{-\infty}^{+\infty} \chi\chi^*(p_x, 0, p_z)\,\mathrm{d}p_x . \tag{2}$$

We denote by P.S. (point slit geometry) this new geometry as opposed to L.S., the previous linear slit geometry. The main disadvantage of P.S. is the very low counting rate resulting from the drastic reduction of the solid angle. It is found, however, that an increase of this rate can be obtained simply by setting in a row, several P.S. slits at equal distances in front of each scintillator.

In such a way the point slits of two scintillators in coincidence result aligned with the target, in pairs (Fig. 1*b*).

In consequence of what we said before, every line joining a pair of opposed P.S., must form an angle of $15 \cdot 10^{-3}$ rad at least, with the adjacent line.

With this limitation in mind one can fit four pairs of P.S. on the same scintillators previously used for L.S.

The point slits have been obtained by a superposition of two flat lead bricks, one of them bearing four milled channels (3 mm large $\times$ 2 mm deep). The channels are all converging to the same point, the center of the target, whose dimensions are 4 mm wide $\times$ 40 mm long.

The experimental apparatus, except for the change of slits, is just the same in all his automatic and electronic parts.

3. – Experimental results.

As a first application, measurements have been performed on graphite, a material having a great anisotropy, using both geometries previously described.

We have studied colloidal, oriented flakes, and monocrystal graphite.

Since the studied surface in our experimental apparatus, lies in a horizontal plane (XY), we refer to samples having hexagonal planes parallel to this surface as « horizontal » samples, and to samples with hexagonal planes normal to this surface, as « vertical » ones.

Vertical graphite may be oriented in ZY, or ZX planes.

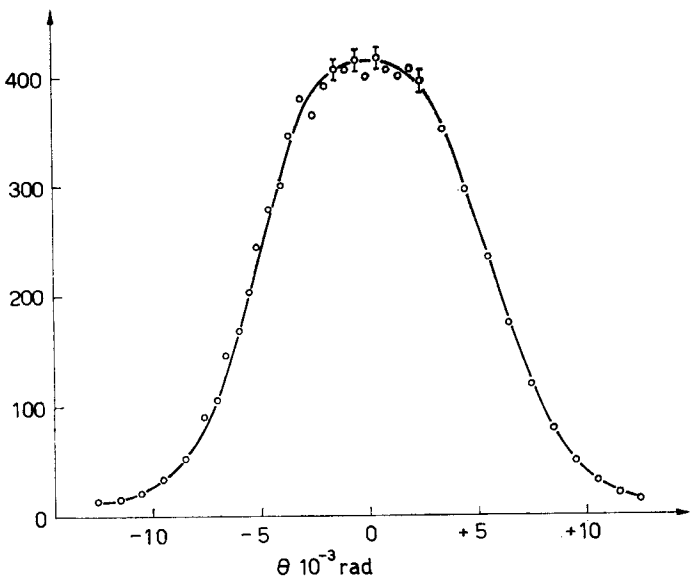

Fig. 2. – Experimental correlation curve (L. S.) from colloidal graphite.

Since polycrystalline samples, obtained by pressing powdered graphite, always present a kind of orientation, we have obtained a sample by depositing a suspension of colloidal graphite.

The oriented samples have been obtained pressing and annealing flakes of graphite.

The last technique, which has been already adopted by other authors [2], makes possible to obtain samples having hexagonal planes oriented parallel to the sample surface.

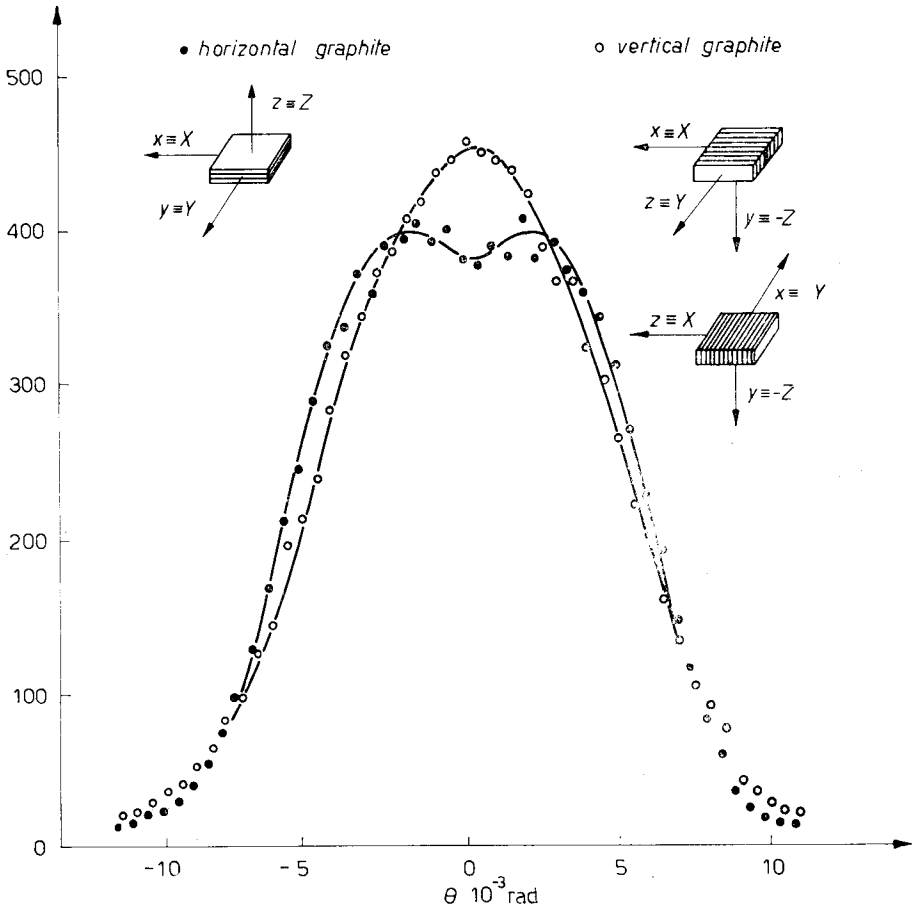

Fig. 3. – Experimental curves (L. S.) from horizontal and vertical graphite.

Samples cut with hexagonal planes perpendicular to the XY plane of our reference system were, on the contrary, obtained from pressed graphite, which was previously embedded in paraffin, since the pressed samples are friable and to cut them along any particular direction, results impossible. The paraffin was then sublimated and the sample annealed.

The annihilation curves Fig. 2, 3, 4, show remarkable differences: the curve resulting from colloidal graphite Fig. 2 looks like a gaussian, while the curve

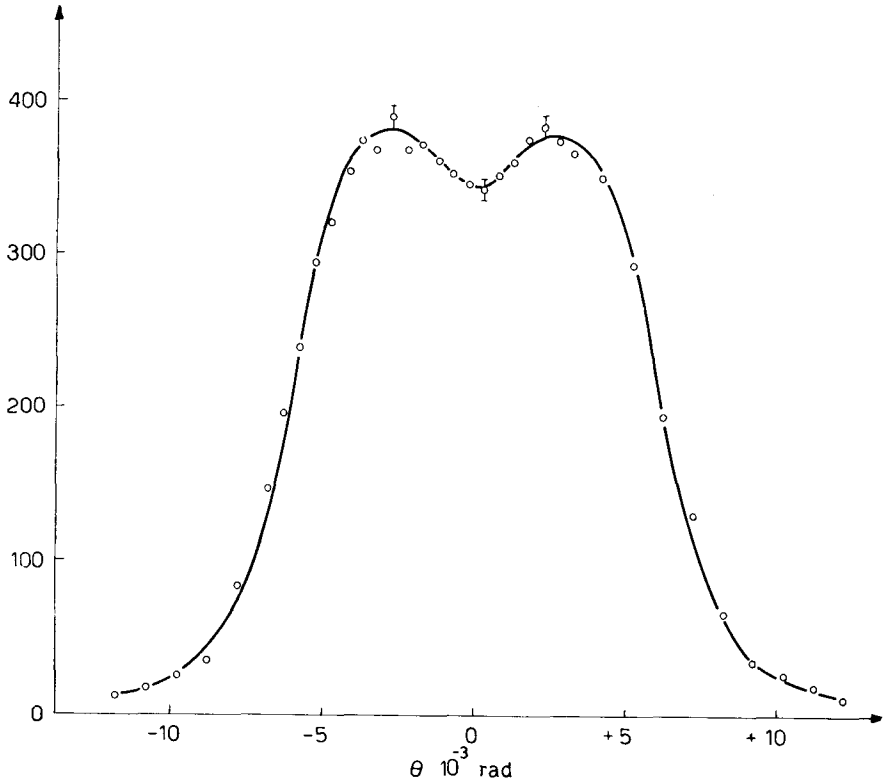

Fig. 4. – Experimental curve (L. S.) from horizontal monocrystal.

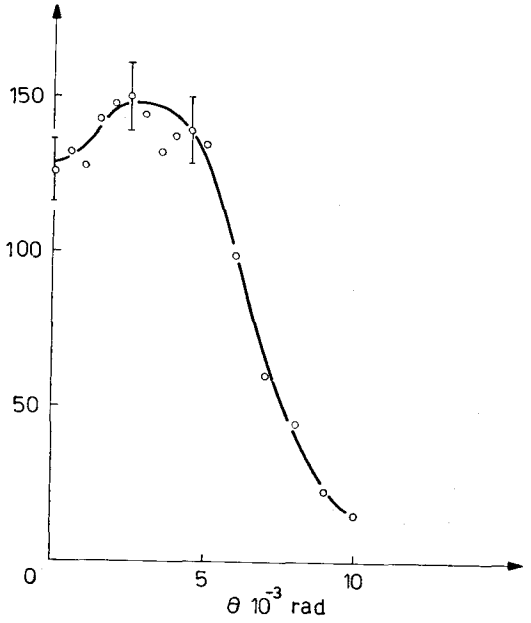

Fig. 5. – Experimental curve (P. S.) from horizontal monocrystal.

from horizontal graphite Fig. 3 presents a central minimum given by π electrons as we shall show later.

The pressed-graphite curve is similar to that obtained by BERKO *et al.* [2] while, the monocrystal curve Fig. 4 shows a more marked minimum, probably because of his better orientation.

In addition we give measurements of the vertical sample Fig. 3 that is peaked with respect

to the colloidal, no difference being observed by orienting hexagonal planes parallel to ZY, ZX planes.

The previous measurements were repeated with P.S. geometry modifying the sample dimensions.

Experimental results on horizontal monocrystal Fig. 5 do not present remarkable difference from the corresponding curve made with L.S.

With the vertical sample two different annihilation curves were obtained, by orienting the normal to hexagonal planes once in the sample-scintillator direction, Fig. 6, and then in the direction perpendicular to the first one and at the same time parallel to the XY plane Fig. 7.

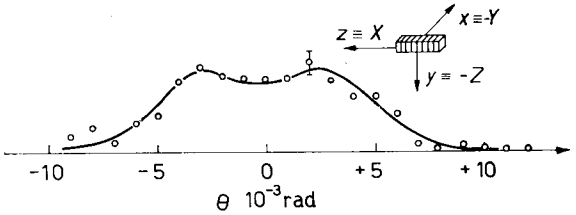

Fig. 6. – Experimental curve (P. S.) from vertical sample with the hexagonal planes normal to the sample-scintillator direction.

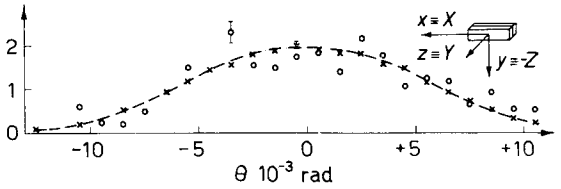

Fig. 7. – Experimental curve (P. S.) from vertical sample with the hexagonal planes parallel to the sample-scintillator direction: (⊙) with ^{22}Na source, (×) with ^{64}Cu source.

4. – Theoretical calculations.

In this section we evaluate by an heuristic method, angular distributions for the different orientations of graphite.

In order to calculate the $\chi\chi^*$ function which appears in (1), (2) and in the other similar expressions referring to various sample-orientations, we have started from the atomic wave function of $2p_z$ state for π electrons and from the wave-function (molecular approximation) relative to σ electrons ([5])

$$\psi_\sigma = \frac{1}{\sqrt{3}} \left[\psi(2s) + \sqrt{2}\,\psi(\sigma_i 2p)\right], \qquad (i = 1, 2, 3), \tag{3}$$

where $\psi(2s)$ is the $(2s)$ wave function for the carbon atom, and $\psi(\sigma_i 2p)$ are the $(2p)$ wave functions whose axes are in the directions σ_i joining the graphite atom to its three neighbours in the plane. We have not taken into account contributions of $1s^2$ electrons.

([5]) P. R. WALLACE: *Phys. Rev.*, **71**, 622 (1947).

From such wave-functions we have deduced the momentum functions using the general procedure given by L. PAULING *et al.* (6).

If one performs the integral for obtaining $N_z(p_z)$ with the hypothesis that σ and π electrons participate to the annihilation in their true numerical ratio (3:1), the curves result, for the horizontal samples, wider than the experimental ones and without the central minimum.

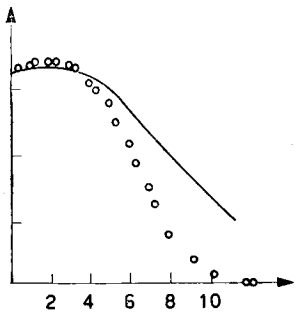

Fig. 8. – Experimental (○) and theoretical (—) curves from pressed horizontal graphite by BERKO *et al.* (2).

On the other hand, a best fit of a linear contribution of the two curves as made by BERKO *et al.* (2) reported in Fig. 8, does not give, as in our case, a good result.

This is a consequence of the fact that, in the $N_z(p_z)$ expressions, one does not take into account the ψ_+ positron wave-function that instead could not be considered constant.

Hence we have followed a procedure which roughly corresponds to introducing in the calculations the effect of the presence of the ψ_+ function. Since ψ_+ vanishes in the neighbourhood of each nucleus, we have excluded from our calculations the contribution of the $\psi(2s)$ component in ψ_σ (formula (3)) and we have at the same time asked that $\chi\chi^*(\boldsymbol{p})$ vanishes more rapidly.

This last condition was obtained by leaving unaltered the functional dependence of $\chi\chi^*$ from its variables, and making a linear change of variable; *i.e.* we have substituted $\chi\chi^*(p, \Theta, \Phi)$ with the new $\chi\chi^*(Kp, \Theta, \Phi)$, $(K>1)$.

This procedure does not seem unreasonable since the positron moves in regions which are far enough from the nucleus.

Finally we take as our space function the linear superposition of ψ_π and ψ_σ:

$$\psi \propto \alpha\psi_\pi + \beta\psi_\sigma ,$$

where α and β are linked by the relation $\alpha^2+\beta^2=1$ which is a consequence of the fact that

$$\int |\psi|^2 \mathrm{d}\tau = \int |\psi_\pi|^2 \mathrm{d}\tau = \int |\psi_\sigma|^2 \mathrm{d}\tau = 1 .$$

Taking the squared modulus of the transform of ψ we obtain:

$$(4) \qquad \chi\chi^*(K\boldsymbol{p}) = \alpha^2\chi\chi_\pi^*(K\boldsymbol{p}) + \beta^2\chi\chi_\sigma^*(K\boldsymbol{p}) + \alpha\beta(\chi_\pi^*\chi_\sigma + \chi_\pi\chi_\sigma^*) \quad (*) ,$$

(6) B. PODOLSKI and L. PAULING: *Phys. Rev.*, **34**, 109 (1929).

(*) The last term of this expression vanishes when performing the integration with respect to the angular variables.

where

$$\chi\chi^*_{\pi}(K\boldsymbol{p}) = A\,\frac{K^2\zeta_z^2}{(K^2\zeta^2+1)^6}\,, \tag{5}$$

$$\chi\chi^*_{\sigma}(K\boldsymbol{p}) = B\,\frac{K^2\zeta_Q^2}{(K^2\zeta^2+1)^6}\,, \tag{6}$$

$$\zeta = (2\pi/\gamma h)mc\cdot 10^{-3}\cdot\vartheta\,; \qquad \zeta^2 = \zeta_x^2+\zeta_y^2+\zeta_z^2\,,$$

$$\gamma = Z - s/na_0\,; \qquad \zeta_Q^2 = \zeta_x^2+\zeta_y^2\,,$$

$$Z - s = 3.25\ (^7),$$

a_0 = first Bohr-orbit radius,

n = principal quantum number = 2.

A and B are choosen so that the integrals of $\chi\chi^*_{\pi,\sigma}$ are normalized to unity.

In the expression (6) we have performed the cylindrical average since the hexagones on the planes are oriented at random and the contribute of $(2s)$ electrons was taken off.

The parameter K was determined, once for ever, for the colloidal-graphite curve, since this curve is not dependent on α^2 [$\alpha^2 = \pi/(\pi+\sigma)$].

Really for this curve the distribution is given by:

$$N_z(p_z) \propto \int_{p_z}^{\infty} \frac{N(p)}{p}\,\mathrm{d}p\,, \tag{7}$$

with

$$N(p) = \int_0^{2\pi}\mathrm{d}\Phi\int_0^{\pi}\mathrm{d}\Theta\cdot\chi\chi^*(p,\,\Theta,\,\Phi)p^2\sin\Theta\,,$$

or

$$N(Kp) \propto \frac{(K\zeta)^4}{(K^2\zeta^2+1)^6}\,(\alpha^2+\beta^2) \qquad \alpha^2+\beta^2 = 1\,. \tag{8}$$

$N(p)\,\mathrm{d}p$ being the number of γ pairs whose momentum has a magnitude between p and $p+\mathrm{d}p$. We have then evaluated K by imposing that the theoret-

---

(7) J. C. SLATER: *Phys. Rev.*, **37**, 57 (1930).

ical and experimental curves (both normalized to the same area) have the same value for $p_z = 0$.

In Fig. 9 both curves are plotted.

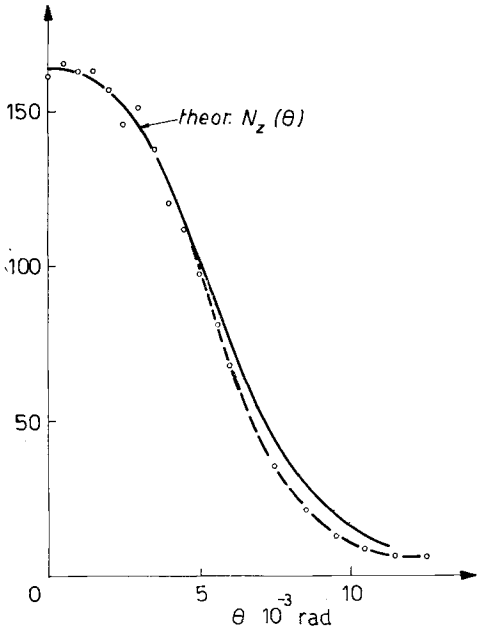

Fig. 9. – Comparison of theoretical (—) and experimental (○) (L. S.) curve for colloidal sample.

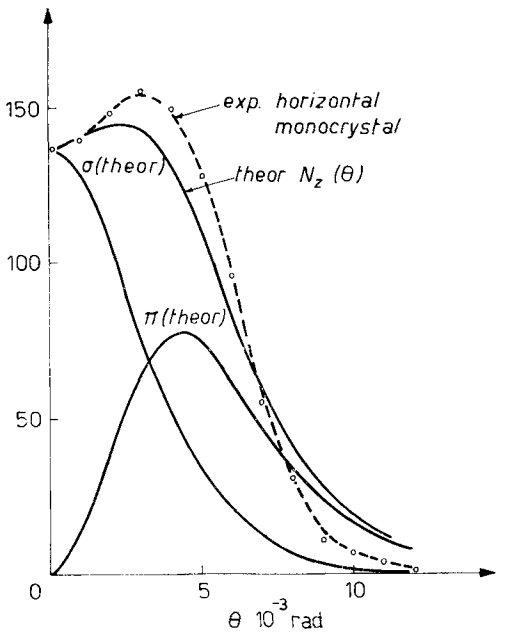

Fig. 10. – Theoretical and experimental (L. S.) distributions for monocrystal sample.

We have determined α^2 in the horizontal monocrystal curve, requiring as before that the theoretical and experimental curves, normalized at 1, have the same value at $p_z = 0$.

We have determined by this procedure the percentage of π electrons which take part in the annihilation, which results to be 48%.

We have plotted in Fig. 10 the theoretical distribution curve, the two components π, σ and the experimental one.

Going further and using always the same value of K and α^2 we have calculated the other curves.

One can notice (Fig. 2, 3, 4) that the colloidal graphite curve is comprised between horizontal and vertical ones, and that the theoretical distribution calculated with formula (8) seems in good agreement with the experimental curve Fig. 9.

The experimental curves from horizontal samples, with both geometries look similar. The comparison with the theoretical curves, calculated intro-

ducing (5), (6) expressions in formula (1) for L.S. and in (2) for P.S., results in Fig. 10, 11, 12. The minimum derives from the shape of formula (5) whose integral vanishes at $p_z = 0$.

What we consider rather interesting is the presence of a central minimum also in the vertical graphite Fig. 6 P.S., minimum that is not found using L.S. as appears from Fig 3.

To calculate the theoretical distribution for vertical samples

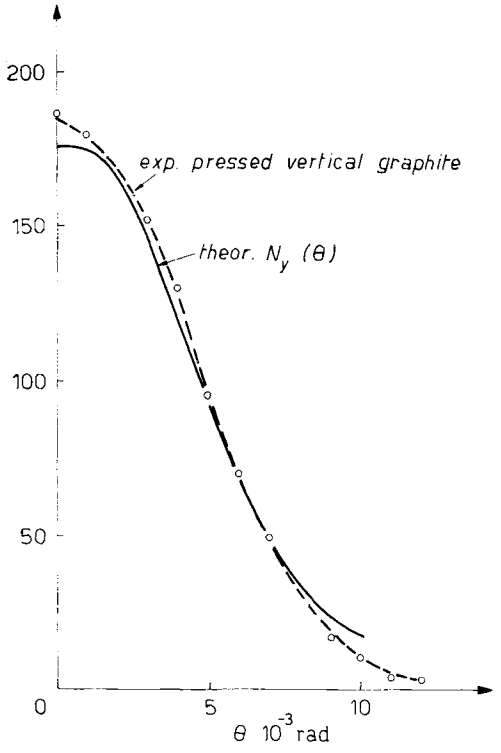

Fig. 11. – Theoretical and experimental curves (L. S.) for vertical sample.

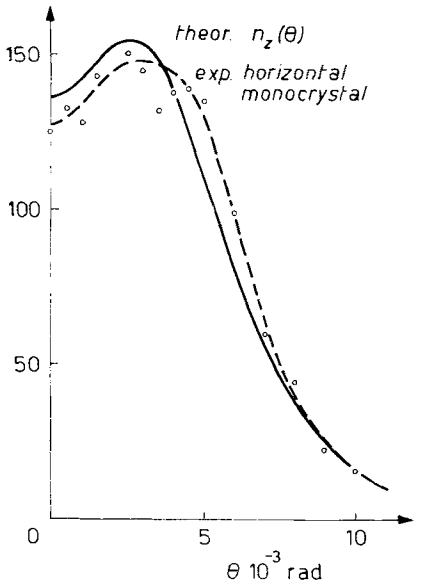

Fig. 12. – Theoretical and experimental curves (P. S.) for monocrystal sample.

Fig. 11, 13*a*, 13*b* we have substituted formulas (5), (6) in

(9) $$N_y(p_y) \propto \int\int_{\infty} \chi\chi^*(p_x, p_y, p_z)\, \mathrm{d}p_x\, \mathrm{d}p_z\,, \qquad \text{S.L.}$$

(10) $$n_y(p_y) \propto \int_{-\infty}^{+\infty} \chi\chi^*(0, p_y, p_z)\, \mathrm{d}p_z\,,$$

P.S.

(11) $$n_{y0}(p_y) \propto \int_{-\infty}^{+\infty} \chi\chi^*(p_x, p_y, 0)\, \mathrm{d}p_x\,,$$

respectively.

Theoretical curve Fig. 13*a* shows that this minimum depends on the contribute of σ electrons in the $(2p)$ state.

Let us notice that we could not obtain this minimum in the theoretical curve of Fig. 13*a* if we had not eliminated the σ electrons in the state $(2s)$.

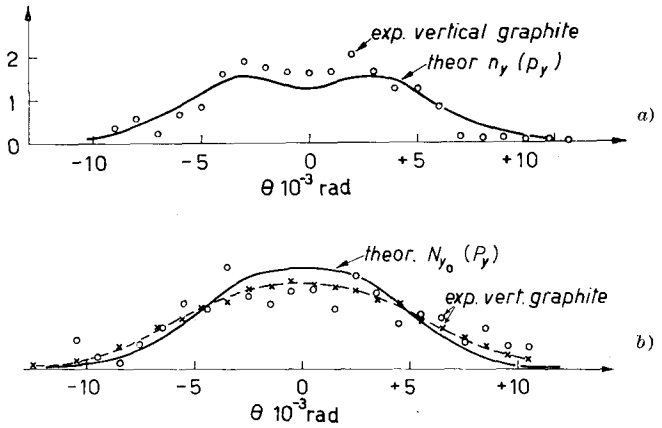

Fig. 13. – *a*) Theoretical and *b*) experimental (P. S.) for both vertical orientations.

The last orientation of the sample should be of great help for the study of σ electrons distribution since as one can observe in formula (11) the π electrons do not occur.

The experimental curve (○) of Fig. 7 is less accurate than the others: therefore we report later measurements (×) made with a more powerful source (300 mC ^{64}Cu). In these curves the central minimum does not appear, in agreement with the theoretical curve of Fig. 13*b*.

* * *

We wish to thank Dr. L. FAVELLA and Prof. P. BROVETTO for some valuable suggestions and discussions.

RIASSUNTO

Si descrive un nuovo dispositivo sperimentale per studiare la distribuzione angolare dei raggi γ di annichilamento dei positoni; il numero di coincidenze $N_z(p_z)$, da esso registrato è proporzionale ad un integrale semplice della funzione densità degli impulsi, mentre con il precedente apparecchio era proporzionale ad un integrale doppio. Sono discussi i risultati delle misure eseguite su campioni di grafite orientati in varie direzioni.